

Title: Vibration Measurement of an Unbalanced Metallic Shaft Using Electrostatic Sensors

Authors: Kamel Reda
Yong Yan

Addresses: School of Engineering and Digital Arts
University of Kent
Canterbury
Kent CT2 7NT
UK
Tel: 00441227823015
Fax: 00441227456084
Email: kr314@kent.ac.uk; y.yan@kent.ac.uk

ABSTRACT

Vibration measurement of a rotary shaft is essential for the diagnosis and prognosis of industrial rotating machinery. However, the imbalance of a shaft, as quantified through vibration displacement, is the most common cause of machine vibration. The objective of this study is to develop a novel technique through electrostatic sensing for the on-line, continuous and non-contact displacement measurement of a rotary shaft due to imbalance faults. A mathematical model is established to extract useful information about the shaft displacement vibration from the simulated signal in the frequency domain. Experimental tests were conducted on a purpose-built test rig to measure the displacement vibration of the shaft. An eccentric shaft was tested with the output signal from the electrostatic sensor analyzed. The effectiveness of the proposed method is verified through computer simulation and experimental tests. Results obtained indicate that the measurement system yields a relative error of within $\pm 0.6\%$ in the displacement measurement.

Index Terms– Rotating machinery; Fault detection; Vibration; Imbalance; Displacement; Electrostatic Sensors.

I. INTRODUCTION

Vibration measurement of rotary shafts plays a significant part in the condition monitoring of rotating machinery. A variety of mechanical defects, such as shaft imbalance, coupling misalignment and bearing deterioration, may give rise to excessive vibrations that cause machine failure. Imbalance is the most common cause of vibrations of rotating machines. In practice, shafts can never be perfectly balanced because of manufacturing errors such as porosity in casting, non-uniform density of material, manufacturing tolerances and gain or loss of material during operation. An unbalanced shaft makes it more susceptible to high amplitude vibrations that cause noise and incorrect functionality and thus reduces the life span of the machine.

There are a range of techniques available for shaft vibration detection through the measurement of displacement, velocity or acceleration [1-4]. However, in certain cases where the mass of the machine casing is much greater than that of the shaft or rotor, conventional contact type sensors such as accelerometers and velocity transducers may not be suitable for detecting the vibration of the shaft [3]. Non-contact type sensors are desirable in such cases. Several types of proximity sensors based on eddy current, ultrasonic, capacitive or inductive principles are often used to measure the relative vibration of a rotating shaft [5, 6]. Recently, a number of new methods have been proposed for shaft vibration detection. Tong et al [7] designed a reflective intensity-modulated non-contact optical fibre sensing system to detect radial vibration of high-speed rotating machinery. Vyroubal [8] identified the vibration signature using optical sensors through spectral analysis of phase-modulated light pulses. Okabe et al [9] described an ultrasonic sensor based method for shaft vibration detection by measuring the propagation time of the ultrasonic wave from the sensor to the shaft surface. Sophisticated optical sensors can be designed to operate in a harsh environment and can perform non-contact displacement measurement with high sensitivity and resolution. However, such devices are prohibitively expensive for routine industrial applications. Much more recently, Wang et al [10] employed electrostatic sensors for the vibration detection of rotating machinery. Later, they proposed a method for the radial vibration measurement of a shaft using electrostatic sensors and Hilbert-Huang Transform [11]. However, both methods were based on the amplitude of the output signal resulting from electrostatic charge on the surface of a rotating dielectric shaft, assuming that the only factor affecting the amount of induced charge and hence the signal amplitude is the distance between the electrode and the shaft. Nevertheless, the electric charge level on the dielectric shaft surface depends significantly on environmental conditions and consequently the signal amplitude varies with environmental factors such as ambient temperature and relative humidity [12, 13]. As a result, these methods cannot be used to achieve an absolute displacement measurement due to the uncertain amount of charge on the shaft surface. Moreover, these methods work only on dielectric shafts and require an array of sensors to be installed around the shaft, making the sensor installation practically difficult.

This paper presents a novel technique to measure the vibration caused by an unbalanced shaft by applying a magnitude-independent method in the frequency domain with the use of electrostatic sensors. The proposed method is based on the frequency properties of the sensor signal, rather than its amplitude to quantify the shaft displacement. This method and hence the measurements, are independent of the level of the accumulated charge on the shaft surface, which makes the measurement system more stable and reliable in harsh industrial environments. In addition, the proposed technique can work on metallic shafts and uses only a single electrostatic sensor. The shaft imbalance detection method along with preliminary experimental results was presented at the 2018 International Instrumentation and Measurement Technology Conference [14]. This paper presents in detail the principle of the vibration displacement measurement of an unbalanced shaft along with experimental results. Mathematical modelling of the sensing system is also established to study the frequency response characteristics of an eccentric metallic shaft.

II. MEASUREMENT PRINCIPLE

Fig. 1 shows a simplified physical model of the electrostatic sensing system for displacement measurement. The physical model consists of a metallic shaft, electrically isolated point charges fixed on the shaft surface (e.g. points M and N), an electrostatic electrode and associated signal conditioning circuit.

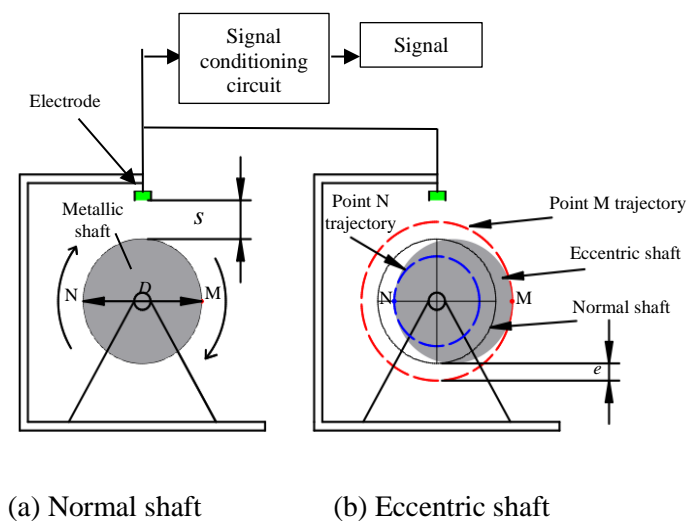


Fig. 1. Physical model of the sensing system.

A small electrostatically charged marker made of electret film with an area of 4 mm^2 is fixed on the metallic shaft. The marker simulates a point charge on the shaft surface. An electrostatic sensor consists of an insulated electrode with a suitable charge detection circuit can detect the charge on the marker and generate an output signal through electrostatic induction. Previous research [15] shows that the frequency response of the sensor output depends primarily on the circular trajectory diameter D of a rotating point charge fixed on the shaft surface (points M or N in Fig. 1), the distance s between the point charge and the electrode, and the angular speed of the shaft. For a given point charge on the shaft, the rotational motion results in a circular trajectory of the point charge. In the case of a normal shaft, the shortest distance between any rotating point on the shaft and the electrode is constant, as is its trajectory diameter, which is equal to D . While each point on an eccentric shaft rotates along a different circular trajectory and results in a variation in the distance s . By analyzing the frequency response of the output signal, the displacement and hence the imbalance of the shaft can be quantified. When n identical markers (e.g. $M_1 \dots M_8$) are fixed around the shaft, the output signal is then composed of n pulses corresponding to the n markers, as shown in Fig. 2.

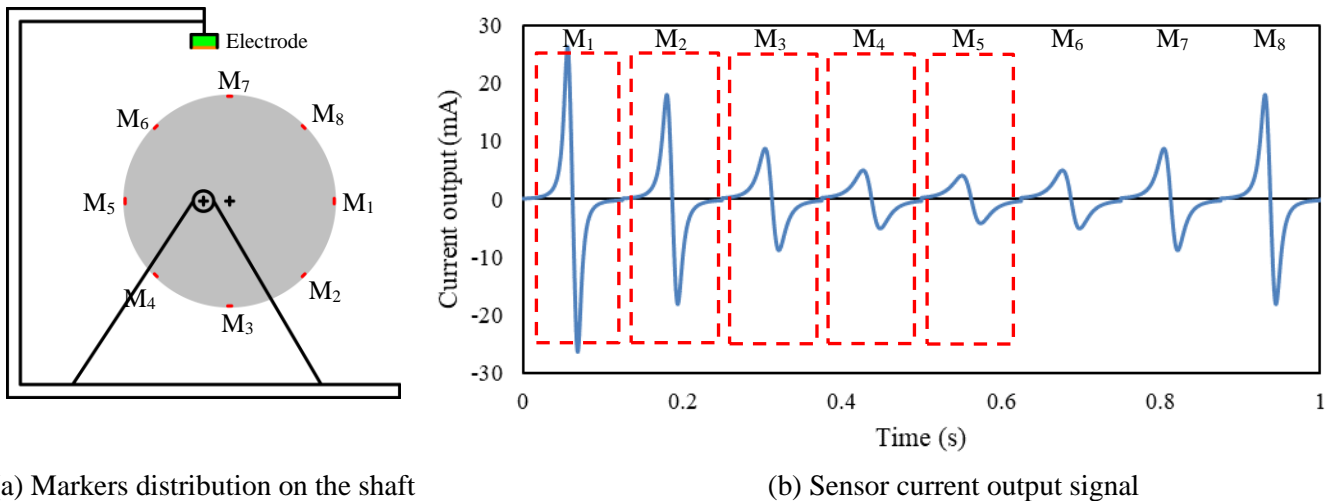


Fig. 2. Distribution of markers on the shaft and corresponding output signal results over one revolution (speed=60 rpm).

It is worth noting that the markers M_1 and M_5 correspond to the shortest and longest distance from the shaft surface to the electrode, respectively (Points M and N in Fig. 1).

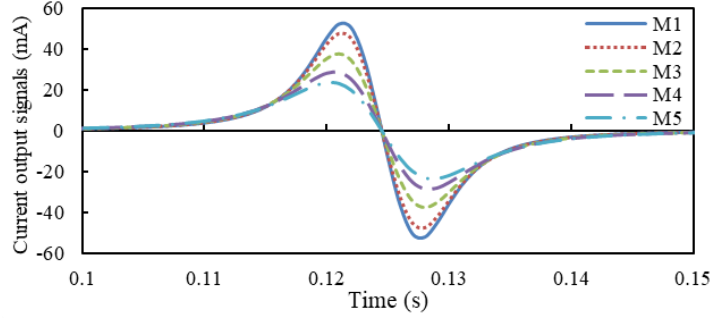


Fig. 3. Decomposition of the output signal into 5 single signals.

It can be seen from Fig. 2 that the distance between M_4 and the center of rotation is equal to that between M_6 and the center of rotation. Similar dispositions exist with respect to points M_3 - M_7 and M_2 - M_8 . Consequently, the pulses resulting, respectively, from M_6 , M_7 - M_8 and M_4 , M_3 - M_2 , are identical. Therefore, it would be sufficient to analyze the first five pulses (M_1 - M_5) which are distributed over the semi-circumference of the shaft. The output signal is first decomposed in the time domain into single pulses corresponding to the markers fixed on specific locations around the shaft. The corresponding spectra are plotted in Fig. 4. However, the decomposition should be performed under the assumption that the pulses resulting from the markers (point charges) do not overlap with each other. Accordingly, the number and arrangement of the markers should be well defined in order to satisfy this condition. The number and arrangement of the markers around the shaft depend primarily on the shaft diameter, angular speed to be measured and the size of the markers.

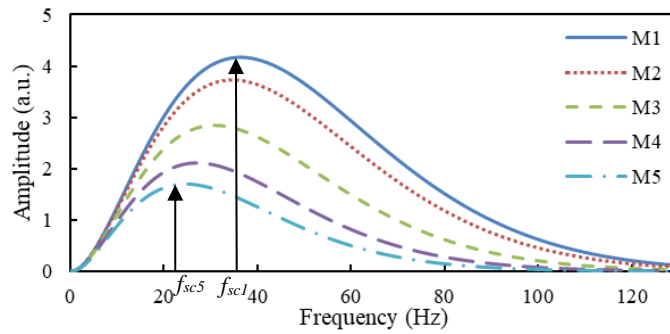


Fig. 4. Amplitude spectra of the decomposed pulses.

Fig. 4 shows that, when a point charge on the shaft surface rotates closer to the electrode (e.g. M_1), the frequency at the spectrum crest (f_{sc1}) has a higher value than that of a point charge rotating farther to

the electrode. When a point charge rotates closer to the electrode, the electrode covers a smaller area of the electric field, and the induction occurs for a shorter period and subsequently gives rise to a signal of higher frequency. As a result, the closer the distance between the electrode and the shaft surface, the more the induced charge on the electrode and the higher the frequency.

The magnitude frequency response of the output signals due to different point charges on an eccentric shaft (different displacements), rotating at a constant speed, shows different frequencies at the peak of spectra or the frequency at the spectrum crest (f_{sc}) (Fig. 4). Therefore, the displacement can be derived from f_{sc} .

III. MATHEMATICAL MODELLING OF THE SENSOR

A. Mathematical Model of the Sensor

A mathematical model of the electrostatic sensing system for the rotational motion of an electrostatic point charge should be established in order to study the sensing characteristics of the sensor. From the developed model, we can derive an analytical relationship between the displacement s and the characteristics of the sensor in the frequency domain. Fig. 5 shows an overview of the sensing arrangement in the mathematical modelling. The circle C in Fig. 5 indicates a cross section of a metallic shaft with a diameter D , on which an electrically insulated point charge is fixed. The rotational motion of the point charge at angular speed ω creates, in effect, an impulse input to the sensing system. A strip type electrode with dimensions $L \times W$, made on a small printed circuit board with adequate insulation together with grounding around the electrode, can be regarded as a piece of perfectly conductive metal and is placed at distance s from the shaft.

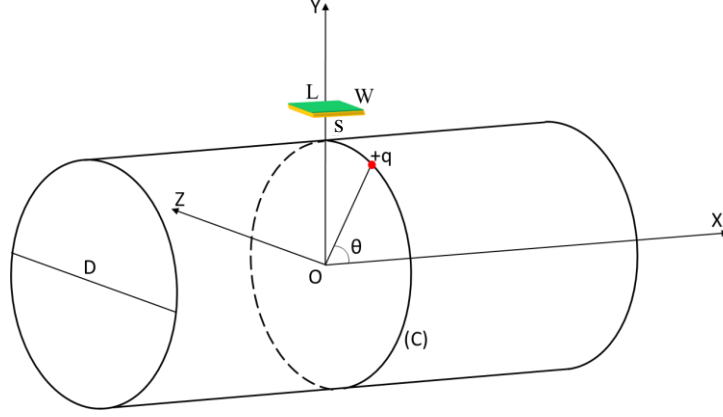


Fig. 5. Electrostatic sensing arrangement in the mathematical modelling.

Based on Gauss's law, the total induced charge Q on the surface of the electrode due to the rotating charge q on the shaft is given by [15]:

$$Q(t) = \frac{-q}{2\pi} \int_{-\frac{W}{2}}^{+\frac{W}{2}} \int_{-\frac{L}{2}}^{+\frac{L}{2}} \frac{0.5D + s - 0.5D \sin \omega t}{((x - 0.5D \cos \omega t)^2 + (0.5D + s - 0.5D \sin \omega t)^2 + y^2)^{\frac{3}{2}}} dy dx \quad (1)$$

Then,

$$Q(t) = \frac{-q}{2\pi} \sum_{i=1}^2 \arctan \left[\frac{0.5L(0.5W + 0.5D\beta_i \cos \omega t)}{(0.5D + s - 0.5D \sin \omega t) \sqrt{(0.5D + s - 0.5D \sin \omega t)^2 + (0.5W + 0.5D\beta_i \cos \omega t)^2 + (0.5L)^2}} \right] \quad (2)$$

Taking D as the basic dimensional unit in the sensing system, W , L and s can all be normalised with reference to D , the total charge becomes:

$$Q(t) = \frac{-q}{2\pi} \sum_{i=1}^2 \arctan \left[\frac{0.5\delta_L(0.5\delta_w + 0.5\beta_i \cos \omega t)}{(0.5 + \delta_s - 0.5 \sin \omega t) \sqrt{(0.5 + \delta_s - 0.5 \sin \omega t)^2 + (0.5\delta_w + 0.5\beta_i \cos \omega t)^2 + (0.5\delta_L)^2}} \right] \quad (3)$$

where $\beta_i = \text{sgn}(i - 1.5)$, $\delta_L = \frac{L}{D}$, $\delta_w = \frac{W}{D}$, $\delta_s = \frac{s}{D}$.

If the electrode is connected to a signal conditioning circuit, as shown in Fig. 6, that converts the induced charge into an induced current, then the actual current output $I_s(t)$ of the sensor is thus:

$$I_s(t) = \frac{dQ(t)}{dt} \quad (4)$$

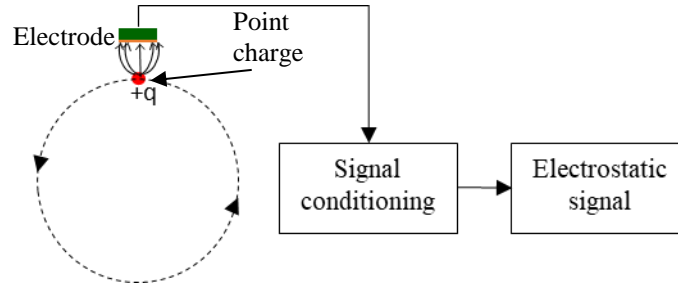


Fig. 6. Simplified model of the sensing system.

B. Impulse and Frequency Response of the Sensor

A point charge approaching towards the electrode along a circular trajectory from infinity is equivalent to an impulse input with amplitude q (i.e. $q\delta(t)$) to the sensing system, thus the impulse response $h_s(t)$ of the system is given by:

$$h_s(t) = \frac{dQ(t)}{qdt} \quad (5)$$

The frequency response of the sensing system can be determined from the Fourier transform of the impulse response $h_s(t)$:

$$H_s(f) = \int_{-\infty}^{+\infty} h_s(t) e^{-j2\pi ft} dt \quad (6)$$

By substituting $h_s(t)$ in equation (5) into equation (6), the amplitude of the frequency spectrum can be written as:

$$|H_s(f)| = F(\omega, D, s) \quad (7)$$

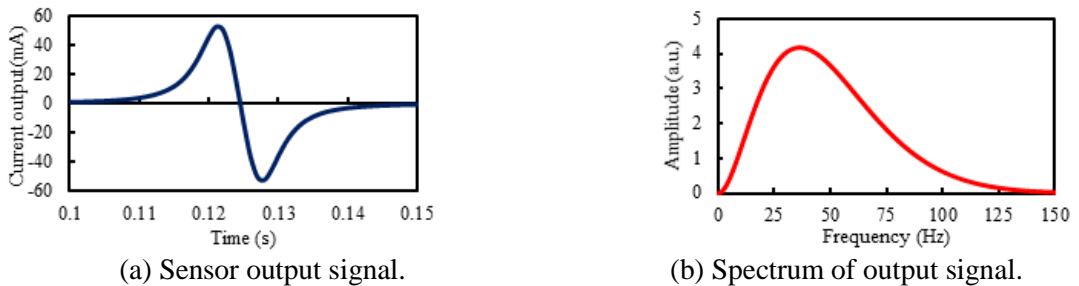


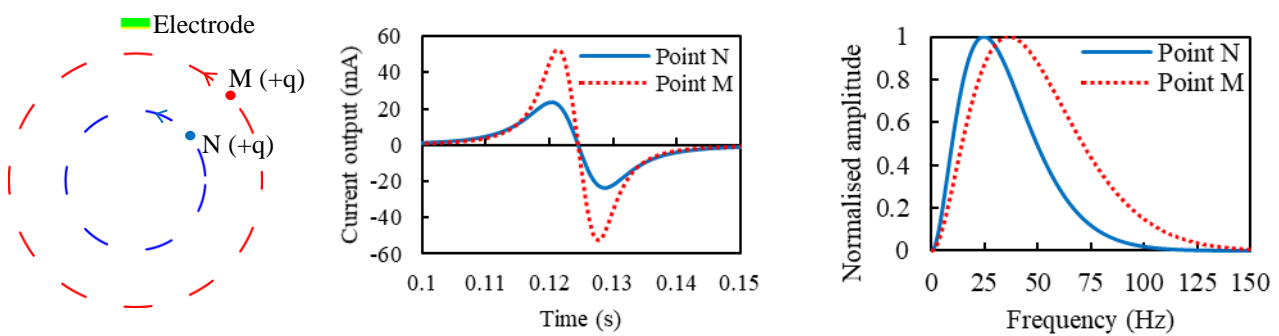
Fig. 7. A typical example of the sensor output and corresponding frequency spectrum.

Equation (7) implies that the amplitude of the spectrum is a function of the angular speed ω , the diameter of the shaft D and the distance s between the shaft surface and the electrode.

C. Displacement effect on the frequency response

The effect of the displacement on the frequency response is investigated for a strip shape electrode [16], using different point charges, with the same magnitude, and rotating along circular trajectories of different diameters (Fig. 8(a)). Subsequently, different trajectories result in different distances to an electrode (displacement), which is located at a fixed distance from the rotation center.

Fig. 8(b) and Fig. 8(c) show the signal outputs of the electrostatic sensor and the corresponding normalised spectra for two different point charges rotating at $\omega=12$ rad/s, which is equivalent to 115 RPM.



(a) Two point charges in rotational motion.

(b) Sensor output signals.

(c) Spectra of output signals.

Fig. 8. Sensor's output of two point charges in rotational motion and its corresponding spectra .

Fig. 8(c) illustrates the output signals in the frequency domain, indicating the effect of the displacement on the frequency characteristics of the sensor. It can be noted that a shorter distance between the electrode and the circular trajectory of the point charge results in more induced charge on the electrode and hence higher signal amplitude (Fig. 8(b)). Moreover, a shorter distance yields a wider bandwidth and a higher frequency at the maximum amplitude (Fig. 8(c)), suggesting that the point charge being within the sensing region of the electrode for a shorter period of time at a constant angular speed.

D. Characteristics of an Unbalanced shaft

1) Vibration of an unbalanced shaft

In general, all rotating machines produce some form of vibration is a function of the machine dynamics such as imbalance, misalignment, bearing deterioration and mechanical looseness [17]. There are three main parameters used to evaluate the vibration characteristics of any dynamic system: displacement, velocity and acceleration [18, 19]. Imbalance is the most common mechanical fault and source of vibration in rotating equipment. Shaft imbalance is a condition in which the centre of mass of the shaft is not coincident with the centre of rotation. A static imbalance is a condition of imbalance where the central principal axis of inertia is displaced in parallel with the axis of rotation, as shown in Fig. 9.

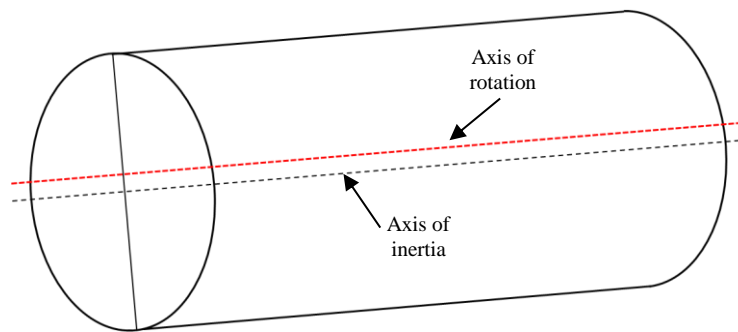


Fig. 9. Static imbalance of shaft in rotating machines.

This paper is concerned with the static imbalance fault which can be determined from the radial vibration of the shaft through instantaneous displacement measurement of the shaft surface with respect to a non-moving reference point.

2) Modelling of the displacement due to static imbalance of a shaft

The vibration due to shaft imbalance can be determined through the displacement measurement of the shaft surface with respect to a fixed position (the sensor). However, it is essential to establish a mathematical model of the shaft displacement. Fig.10 shows the geometrical model of an unbalanced shaft in rotational motion when an electrostatic sensor is used. The simulation results from the mathematical model of the shaft displacement will be used in the regression analysis in order to

develop an estimated regression equation, which gives the displacement as a function of the frequency at the spectrum crest (f_{sc}). Additionally, the modelling results will be used to evaluate the accuracy of the regression model. The model is established with the following assumptions:

- An electrode is placed on the Y-axis, at distance ($R_0 + s_0$) from the X-axis. The position of the sensor is considered as a fixed reference.
- The circle with diameter $2R_0$ represents a cross section of a metallic shaft.
- The rotation center O' of the circle is offset from the geometric center O by the distance e .

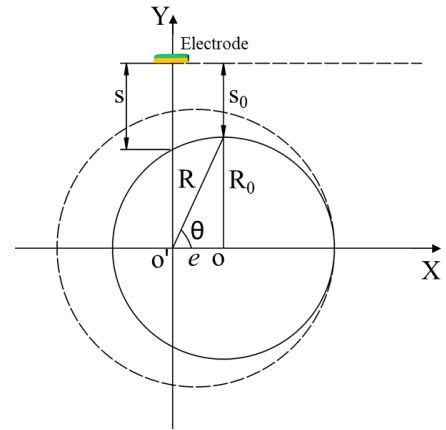


Fig. 10. An unbalanced shaft.

- The rotational motion of the circle about the center O' simulates an unbalanced shaft.
- The shaft and hence the circle is rotating at a constant angular speed $\omega = \theta / t$.
- The displacement s is the distance between the shaft surface and the sensor.
- The eccentricity e with respect to the radius R is relatively small ($e \ll R$).

From Fig. 10, R_0 is given by:

$$R_0^2 = R^2 + e^2 - 2eR \cos \theta \quad (8)$$

Rearranging equation (8):

$$R = e \cos \theta + \sqrt{e^2 \cos^2 \theta - e^2 + R_0^2} \quad (9)$$

As the sensor is located at a fixed distance from the X-axis, then:

$$R_0 + s_0 = R + s \quad (10)$$

By substituting R from equation (9) to from equation (10), the shaft displacement with respect to the sensor position can then be determined by:

$$s = R_0 + s_0 - e \cos \theta - R_0 \sqrt{1 - \frac{e^2}{R_0^2} \sin^2 \theta} \quad (11)$$

As $e \ll R$, then the displacement can be approximated by:

$$d(\theta) = s_0 - e \cos \theta \quad (12)$$

Since $\theta = \omega t$, equation (12) can be rewritten as:

$$s(t) = s_0 - e \cos \omega t \quad (13)$$

where s_0 denotes the distance between the sensor and the normal shaft and e the eccentricity of the shaft.

Equation (13) implies that the displacement of an unbalanced shaft with respect to a fixed position could be approximated to a sinusoidal waveform, as illustrated in Fig.11.

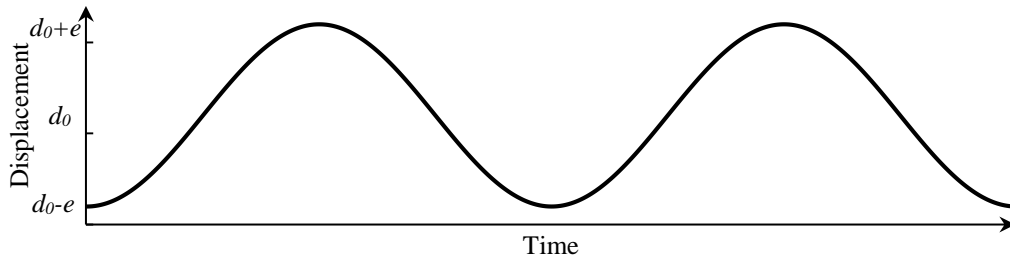


Fig. 11. Displacement function of an eccentric shaft.

E. Estimation of the displacement function of an eccentric shaft

Equation (7) defines the spectrum of the output signal as a function of ω , s and D . For a rigid shaft supported on rigid bearings, the shaft displacement is independent of the shaft angular speed [3]. Previous research demonstrates that the bandwidth is proportional to the angular speed [15]. Subsequently, the frequency at the spectrum crest f_{sc} has a linear relationship with the angular speed. Moreover, the diameter D of each point on the eccentric shaft has a direct relationship with the

displacement ($D + s = K$), where K is a constant (Fig. 1). Thus, the frequency of the spectrum crest f_{sc} can be normalised to the angular speed and can be expressed as a function of the displacement s :

$$f_{sc\perp} = \frac{f_{sc}}{\omega} = F(s) \quad (14)$$

From equation (14), the displacement could be determined analytically as a function of the normalized frequency of the spectrum crest:

$$s = F^{-1}(f_{sc\perp}) \quad (15)$$

The frequency at the spectrum crest is determined where the spectrum amplitude slope is equal to zero:

$$\frac{d(|H_s(f)|)}{df} = 0, \text{ at } f=f_{sc} \quad (16)$$

However, the analytical solution to equation (16) is very complex, a polynomial regression analysis is thus used instead to estimate the relationship between the two variables, the displacement s and f_{sc} .

From Table 1, the displacement s can be estimated as:

$$s = p_3 \cdot f_{sc\perp}^3 + p_2 \cdot f_{sc\perp}^2 + p_1 \cdot f_{sc\perp} + p_0 \quad (17)$$

where $p_0=0.00916$; $p_1=-0.006206$; $p_2=0.001786$; $p_3= -0.0001922$; $f_{sc\perp} = \frac{f_{sc}}{\omega}$.

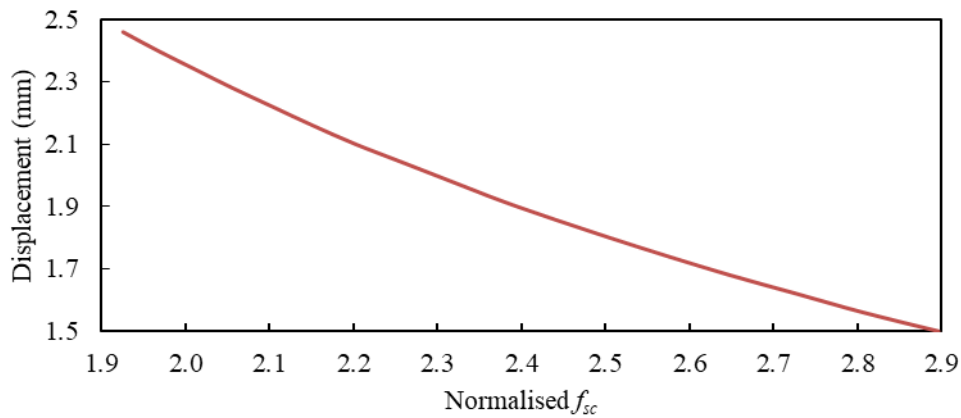


Fig. 12. Relationship between displacement and normalized f_{sc} .

TABLE 1. $f_{sc\pm}$ at different displacements and diameters

s (mm)	D (mm)	Θ (rad)	$f_{sc\pm}$	Fit std. error
1.50	60.50	1.57	2.90	-0.16%
1.56	60.44	1.67	2.81	0.05%
1.62	60.38	1.76	2.73	-0.03%
1.68	60.32	1.86	2.65	0.05%
1.74	60.26	1.96	2.58	0.01%
1.80	60.20	2.05	2.51	-0.01%
1.86	60.14	2.15	2.44	0.00%
1.92	60.08	2.25	2.37	0.03%
1.98	60.02	2.34	2.32	-0.11%
2.04	59.96	2.44	2.26	-0.10%
2.10	59.90	2.54	2.20	0.07%
2.16	59.84	2.63	2.15	0.03%
2.22	59.78	2.73	2.10	-0.06%
2.28	59.72	2.83	2.06	-0.03%
2.34	59.66	2.92	2.01	-0.07%
2.40	59.60	3.02	1.97	0.00%
2.46	59.54	3.11	1.93	-0.02%

For an eccentricity of 0.5 mm ($\delta_e=1/120$) and $\omega =100$ rad/s (955 RPM), the displacement fluctuation is 1 mm, resulting in a variation in f_{sc} of 100 Hz (simulated result). Hence, the measurement sensitivity is 0.01 mm/Hz. If the signal is acquired over one second, then the measurement resolution would be 0.01 mm.

Using equation (17), displacement values can be estimated for each f_{sc} . It can be seen from Fig. 13 that the displacement distribution of an eccentric shaft is similar to a sinusoidal distribution function, which agrees with the displacement function of an unbalanced shaft. At a given angular speed ω , the distribution of s can be fitted to a sinusoidal function. Hence, the displacement function can be written as:

$$s(t) = A \cos \omega t + B \quad (18)$$

where $A = -e$, which denotes the eccentricity of the shaft and is unknown and $B = s_0$ which is a constant representing the displacement of a normal shaft.

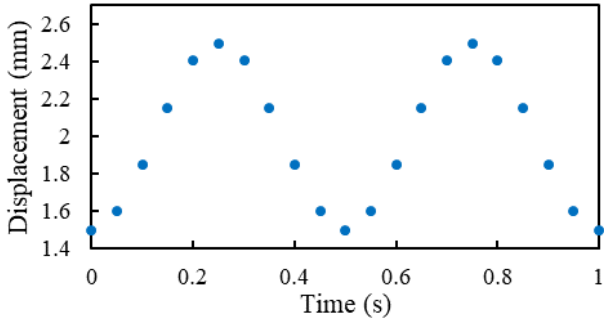


Fig. 13. Displacement values over 2 revolutions.

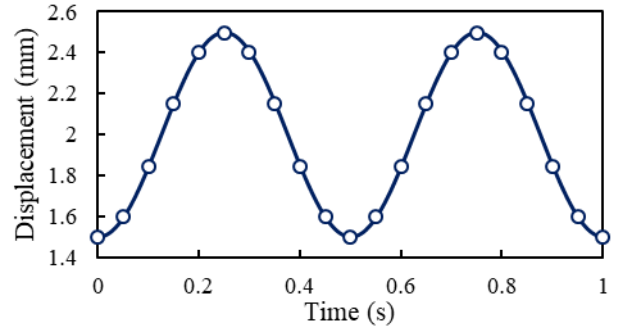
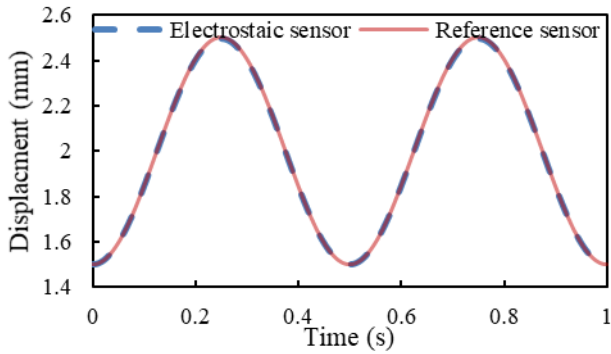
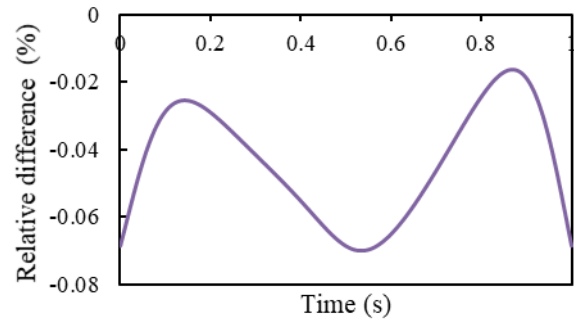


Fig. 14. Fitted curve of the displacement distribution.



(a) Comparison of displacement measurements



(b) Relative difference

Fig. 15. Comparison of the displacement measurement and the relative difference between the electrostatic sensor and the simulated reference.

Fig. 15 shows a comparison between the reference simulation results and the modeling results. It is evident that the mathematical modeling results follow closely the reference simulation results, and the small discrepancy is due to the curve fitting errors.

As a result, the property of the electrode in the frequency domain, being the frequency at the spectrum crest f_{sc} , has been used to establish a method to measure the instantaneous displacement of the shaft and hence the vibration of an unbalanced shaft is quantified.

IV. EXPERIMENTAL RESULTS AND DISCUSSION

A. Experimental Set-up

The electrostatic sensor was designed and fabricated based on a double-sided printed circuit board (PCB). As shown in Fig.17, the electrode is a 4-mm wide tin-plated copper strip embedded in the bottom layer of the PCB. The area around the electrode is filled with earthed copper to minimise the

influence of external electromagnetic interferences. On the top layer of the PCB is the signal conditioning circuit. The current signal from the electrode is first converted into a proportional voltage signal using an I - V converter. To maximize the power transfer between the electrode and the signal conditioning circuit, a FET amplifier is chosen for I - V conversion. Then the bipolar signal is further amplified and level shifted using a high-accuracy instrumentation amplifier to match the input range of a single-supply A/D converter. The instrumentation amplifier also provides an adjustable gain for the circuit using a potentiometer. Finally, a Sallen-Key low-pass filter is used to remove high frequency noise from the sensor output and provide anti-aliasing in the A/D conversion. The sensor is shielded with an earthed metal screen to reject external electromagnetic interferences. Fig. 16 shows the block diagram of the signal conditioning circuit. The output sensor signal was sampled at a frequency of 50 kHz using a data acquisition device (National Instruments, model USB-6341) and processed on a host computer. A bespoke software system was developed using LabView in order to achieve on-line displacement measurement.

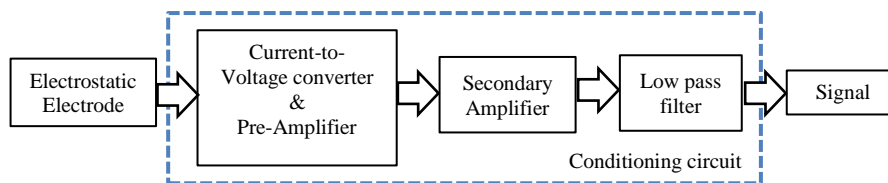
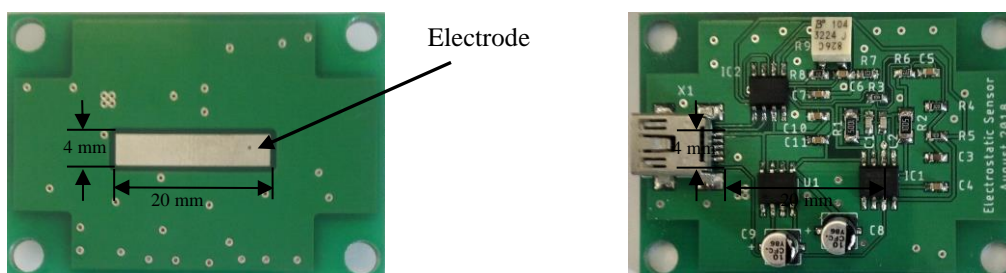


Fig. 16. Block diagram of the conditioning circuit



(a) Electrode layer

(b) Components layer

Fig. 17. Electrostatic sensor and signal conditioning circuit.

Experimental tests were conducted on a purpose-built test rig as shown in Fig. 16 to validate the performance of the electrostatic sensor for vibration displacement measurement against a reference

displacement sensor. The rotational speed of the motor is adjustable through the motor controller. A commercial laser based tachometer (Monarch Instruments, PLT200) was used to obtain reference speed of the shaft. An eccentric metallic shaft with a diameter of 60 mm and an eccentricity of 0.5 mm from the rotation axis was tested. An electrostatic sensor (Fig. 17) was placed 2 mm away from the shaft surface. To simulate eight point charges on the rotor surface, eight charged markers, each being made from 2x2 mm² electret material film, were fixed evenly along the circumference of the eccentric shaft. Two of them were located at the shortest and longest distance with respect to the centre of rotation. Electrets are dielectrics that have a quasi-permanent electrostatic charge. The electret markers were fabricated through a typical micro fabrication process using Teflon FEP films (Fluorinated Ethylene Propylene). The FEP film with a thickness of 127µm was charged with the use of a point-to-plane corona discharge. After charging, the surface potential of the FEP electret film reaches -560 V [20, 21]. The output of the sensor, resulting from the induced charge on the electrode, is derived and measured. Then, the frequency response of the output signal is obtained. A displacement sensor of eddy current type (Model LD701-2/5, OMEGA) was used as a reference instrument to obtain the relative distance between sensor and the shaft surface. All the tests were conducted in a laboratory with air conditioning (ambient temperature of 22°C and relative humidity of 49%).

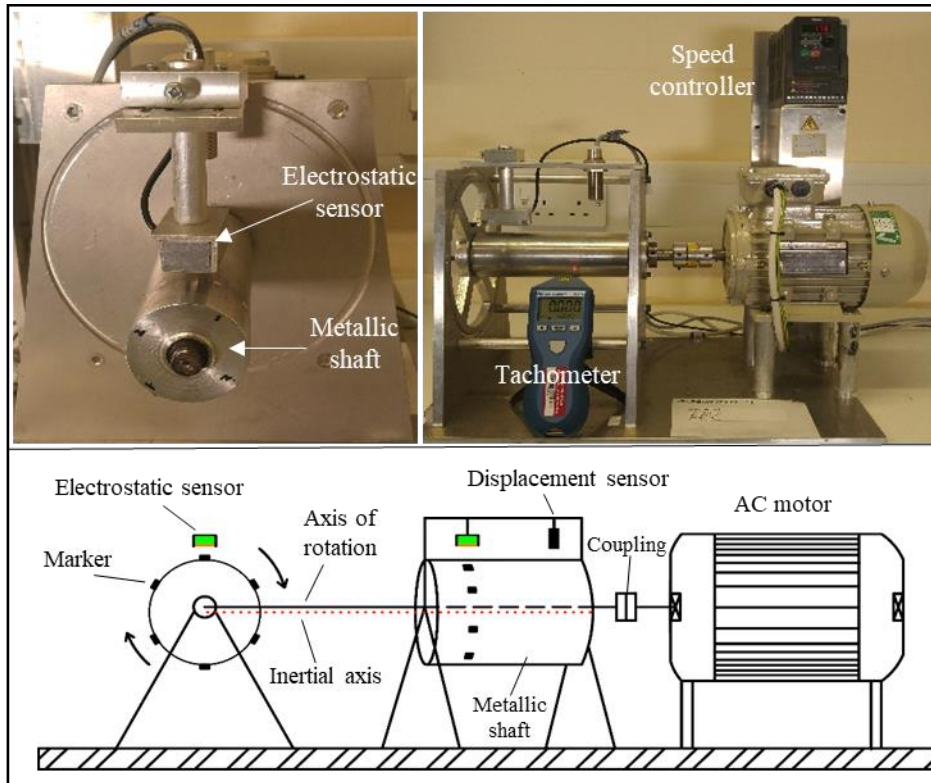


Fig. 18. Test rig.

B. Results and Discussion

A minimum strength of the electrostatic signals has to be maintained to achieve a valid measurement of the displacement using electrostatic sensors. The root mean square (rms) amplitude of an electrostatic signal is used to quantify the signal strength. Previous research shows that if the electrode is moved away from the shaft surface, the effect of electrostatic induction on the electrode is reduced, leading to a weakened signal [15]. In this experiment, the electrostatic sensor was placed 2 mm away from the shaft surface, the RMS signal strength is about 77.25 mV for the signal conditioning unit used. Additionally, the rejection of extrinsic noise due to a near power line (50 Hz) is efficient since an earthed metal screen is used to prevent the interference of electromagnetic fields. However, further investigation is required when applying this technique in an industrial environment with various sources of electromagnetic interference. Fig. 19 shows the output signal from the electrostatic sensor for one period which is the time of the shaft over one revolution.

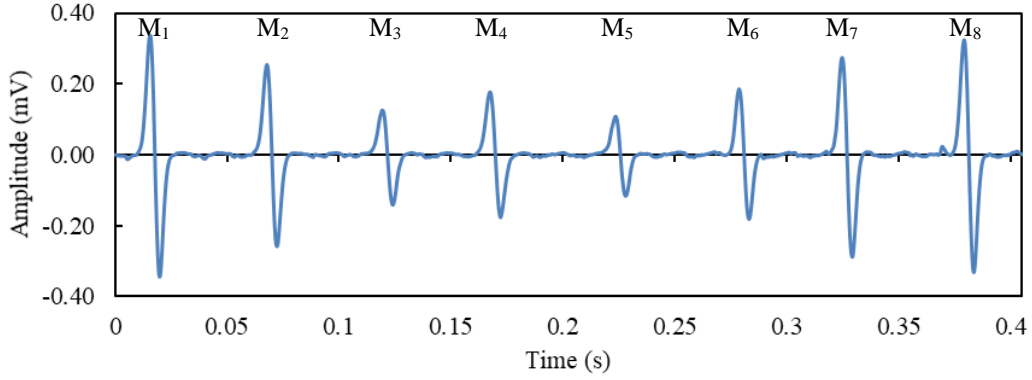


Fig. 19. Output signal from Electrostatic sensor

For each period, the signal is composed by a series of eight pulses resulting from the eight markers on the shaft. It is clear that the amplitude of the signal from the eccentric shaft fluctuates due to the variations in the distance between the shaft and the sensor over one revolution.

Following the measurement methodology in Section III, the signal in Fig. 19 is first decomposed in the time domain into eight single signals corresponding to the eight point charges on the shaft. Then, frequency analysis of each single signal is performed in order to extract the frequency at the spectrum crest f_{sc} . Fig. 20 presents the f_{sc} values of the eight signals for an eccentric shaft ($e = 0.5$ mm) at 148 rpm. Using the regression analysis in Section III, displacement values can be estimated for each f_{sc} . It can be observed from Fig. 21 that the displacement distribution of an eccentric shaft can fit a sinusoidal function, which agrees with the simulation results in Section III.

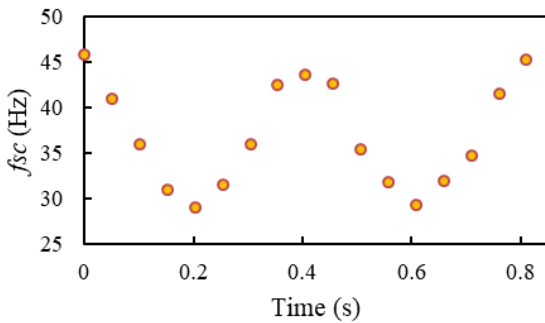


Fig. 20. f_{sc} over 2 revolutions

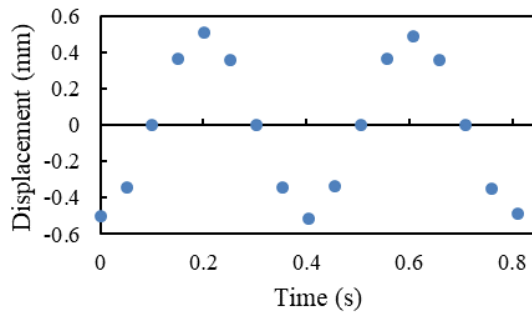


Fig. 21. Estimated displacement values

Fig. 22 presents a direct comparison of the displacement (AC component) of eight points on the eccentric shaft between the electrostatic sensor and the reference sensor (eddy current sensor). The shaft has an eccentricity of 0.5 mm, and is rotating at 148 RPM. All the measured displacements in

Fig. 20 are the average of 20 values with a maximum standard deviation of 4.5 %. It is evident that the measured displacements is pretty close to the reference. Fig. 23 presents that the relative error of the measured displacement is within $\pm 4.2\%$.

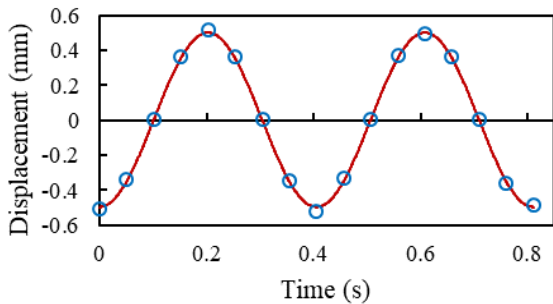


Fig. 22. Comparison between the displacement values and the reference sensor output.

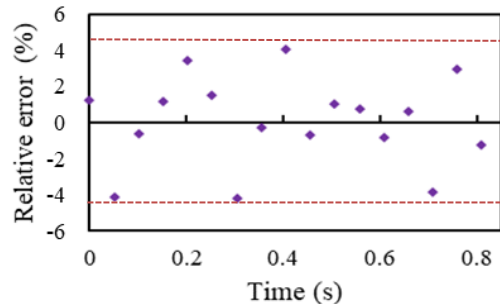
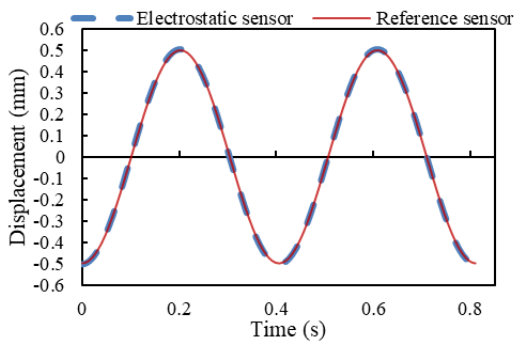
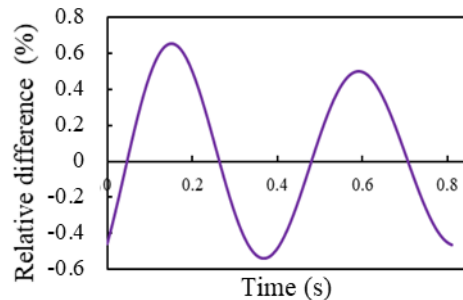


Fig. 23. Relative error from the displacement measurement.

Fig. 24 shows the comparison between the reference and the electrostatic sensor results using a sinusoidal curve fitting. The displacement measurement from the electrostatic sensor in Fig. 24 shows a peak-to-peak displacement of about 1 mm, independent from the rotational speed. The root mean square error (RMSE) between the two displacement curves resulting from the reference sensor and the electrostatic sensor is within 0.77%.



(a) Displacement measurment comparrison



(b) Relative difference

Fig. 24. Comparison of the displacement curve from the electrostatic and the reference sensor.

Fig. 24 (b) shows that the maximum relative error is within $\pm 0.6\%$ compared to $\pm 4.2\%$ of the discrete displacement values (Fig. 23). This result suggests that applying sinusoidal curve fitting to the discrete displacement values with a known frequency (angular speed) has reduced the relative error. It can also

be observed from Fig. 24 (b) that the relative error in the displacement measurement increases when the displacement decreases. The capability of the system to measure smallest displacement values (and hence higher measurement resolution) can be achieved by improving the data acquisition parameters (e.g. sampling frequency, ADC resolution etc.).

V. CONCLUSIONS

The frequency response properties of an electrostatic sensor have been used to detect and quantify an unbalanced shaft through displacement measurement. Experimental results have demonstrated that electrostatic sensors can be used to measure the displacement of an eccentric shaft. Hence, the vibration of an unbalanced shaft can be quantified. Results obtained have demonstrated that the measurement system performs well with a maximum error no greater than $\pm 0.6\%$ under all test conditions. Further research is required to investigate the effect of the markers size and dimensions on the accuracy and repeatability of the measurement. Moreover, the measurement resolution is expected to improve by optimizing the data acquisition parameters. Although, this method has focused on the detection of static imbalance, it can be developed to detect and quantify the two other types of imbalance, i.e. the couple and dynamic imbalance.

ACKNOWLEDGMENT

The authors wish to acknowledge the CEA (Atomic Energy and Alternative Energies Commission) for providing the electret materials in this research.

REFERENCES

- [1] J.Z. Szabo, "Vibration diagnostic test for effect of unbalance," *INES 2012-16th International Conference on Intelligent Engineering System*, pp.81-85 , Lisbon, Portugal, 13-15 June 2012.
- [2] W. Qiao and X. Gong, "Imbalance fault detection of direct-drive wind turbines using generator current signals," *IEEE Trans. Eergy Convers.* vol.27, no 2, pp. 468–476, 2012.

- [3] M. L. Adams, "Rotating machinery vibration: From Analysis to Troubleshooting," New York, USA, CRC Press, 2010.
- [4] R. B. Randall, "State of the art in monitoring rotating machinery-Part 1," *Sound Vib.*, vol.38, no.3, pp. 14-21, 2004.
- [5] H. Chaurasiya, "Recent trends of measurement and development of vibration sensors," *Int. J. Comput. Sci. Iss.*, vol.9, no.4, pp.1694-0814, 2012.
- [6] R. Atashkhomei, J. Urresty, S. Royo, J. Riba and L. Romeral, "Runout tracking in electric motors using self-mixing interferometry," *IEEE/ASME Trans. Mech.*, vol.19, no.1, pp. 184-190, 2014.
- [7] Q. Tong, H. Ma, L. Liu, X. Zhang and G. Li, "Key technology study on radial vibration system of high-speed rotating machinery," *Chinese Journal of Scientific Instrument*, vol.5, no.32, pp. 1026-1032, 2011.
- [8] D. Vyroubal, "Optical method for instant estimate of vibration signature based on spectrum analysis of phase-modulated light pulses," *IEEE Trans. Instrum. Meas.*, vol.53, no.1, pp. 181-185, 2004.
- [9] S. Okabe and S. Tanaka, "Measurement of shaft vibration using ultrasonic sensor," in *Proc. of SICE 2003 Annual Conference*, pp. 1155-1158, Fukui, Japan, 4-6 Aug. 2003.
- [10] L. Wang, Y. Yan, Y. Hu and X. Qian, "Intelligent condition monitoring of rotating machinery through electrostatic sensing and signal analysis," in *proc. of IEEE International Conference on Smart Instrumentation, Measurement and Applications (ICSIMA)*, Kuala Lumpur, Malaysia, 25-27 Nov. 2013.
- [11] L. Wang, Y. Yan, Y. Hu and X. Qian, "Radial vibration measurement of rotary shafts through electrostatic sensing and Hilbert-Huang transform," in *Proc. IEEE International Instrumentation and Measurement Technology Conference (I2MTC 2016)*, pp. 867-871, Taipei, Taiwan, 23-26 May 2016.

- [12]J. Lowell and A. Brown, "Contact electrification of chemically modified surfaces," *J. Electrostat.*, vol.21, pp. 69-79, 1988.
- [13]W. Greason, "Investigation of a test point for triboelectrification," *J. Electrostat.*, vol.49, pp. 245-256, 2000.
- [14]K. Reda and Y. Yan, "Online continuous detection of an unbalanced metallic shaft using electrostatic sensors," in *Proc. IEEE International Instrumentation and Measurement Technology Conference (I2MTC 2018)*, pp. 2073-2078, Houston, USA, 14-17 May 2018.
- [15]L. Wang and Y. Yan, "Mathematical modelling and experimental validation of electrostatic sensors for rotational speed measurement," *Meas. Sci. Technol.*, vol.25, no.11, pp.115101, 2014.
- [16]K. Reda and Y. Yan, "A comparative study of different shaped electrostatic sensors for rotational speed measurement," in *Proc. IEEE SENSORS*, pp. 819-821, Glasgow, UK, 29 Oct.-1 Nov. 2017.
- [17]J. Broch, "Mechanical Vibration and Shock Measurements," Copenhagen, Denmark, Brüel & Kjær, 1984.
- [18]M. MacCamhaoil, "Static and Dynamic Balancing of Rigid Rotors," Copenhagen, Denmark, Brüel & Kjær, 1984.
- [19]F. Fahy, D.Thompson, "Fundamentals of sound and vibration," New York, USA, CRC Press, 2016.
- [20]S. Boisseau, G. Despesse and A. Sylvestre, "Optimization of an electret-based energy harvester," *Smart Materials and Structures*, vol.19, no.7 pp. 075015, 2010.
- [21]S. Boisseau, G. Despesse and B. Ahmed Seddik, "Electrostatic conversion for vibration energy harvesting" (Chapter 5), *Small-Scale Energy Harvesting* (Mickael Lallart), Rijeka, Croatia, IntechOpen, 2012.